

Docking and molecular dynamics simulations of ORPphilins targeting OSBP

Zoé Grimanelli, Bruno Mesmin*, and Romain Gautier

Institut de Pharmacologie Moléculaire et Cellulaire, Université Côte d'Azur, Inserm, CNRS, Valbonne, France

*Corresponding author. e-mail address: mesmin@ipmc.cnrs.fr

Contents

1. Introduction	2
2. Methods	4
2.1 Equipment	4
2.2 Before you begin	4
2.3 Step-by-step method details: Docking	6
2.4 Step-by-step method details: MD simulations	12
2.5 Analysis	17
2.6 Limitations and validation	23
3. Transparency statement	24
Acknowledgements	24
Appendix A. Supporting information	24
References	24

Abstract

Oxysterol-bind protein (OSBP) mediates cholesterol/phosphatidylinositol-4-phosphate (PI4P) exchange between subcellular compartments, thereby contributing to numerous cellular processes and being linked to several diseases such as cancer and viral infections. Its lipid transfer activity relies on the ORD domain, which forms a hydrophobic pocket enabling binding of sterols and PI4P. Natural compounds from the ORPphilin family have emerged as promising antiviral agents, by targeting the OSBP ORD. However, their functioning at the molecular level remains poorly documented. In this chapter, we detail molecular modelling approaches that offer a valuable tool for exploring these interactions, as they provide dynamic insights into protein–ligand complexes not captured by crystallography alone, while being much faster to obtain. With docking and molecular dynamics (MD) simulations methods, one can predict ORPphilin orientations within the ORD pocket, visualize the complexes, and identify specific binding residues, which could serve as basis for designing mutagenesis experiments. MD simulations can further reveal differences in binding energies among ORPphilins, thereby providing mechanistic insights and rationalization of experimental observations.



1. Introduction

Human Oxysterol-binding protein (OSBP), the first discovered member of the larger OSBP-related proteins (ORP)/OSBP homology proteins (Osh) family, plays a key role in several essential cellular functions (Olkkonen & Ikonen, 2024). OSBP has been extensively studied at structural, biochemical and functional levels, making it a prototypical and well-characterized lipid-transfer protein within the cell (de la Mora et al., 2021; Mesmin et al., 2013, 2017). It contains a conserved OSBP-related domain (ORD), which forms a hydrophobic pocket that specifically accommodates sterols molecules, such as oxysterols and cholesterol, and phosphatidylinositol-4-phosphate (PI4P) (Delfosse et al., 2020). OSBP is also equipped with membrane-targeting regions (PH domain, FFAT motif) allowing it to bridge two organelle membranes simultaneously, mainly the endoplasmic reticulum (ER) and the *trans*-Golgi network (TGN). This physical connection enables a lipid counter-exchange mechanism, where OSBP takes up cholesterol from the ER, delivers it to the Golgi membrane, and in return, extracts PI4P from the Golgi and transports it back to the ER (Mesmin et al., 2013). By regulating PI4P levels and cholesterol gradients, OSBP acts as a signaling hub controlling multiple key cellular processes (Appu et al., 2025; Kovács et al., 2024; Lim et al., 2019; Malek et al., 2021; Tan & Finkel, 2022). Of note, lipid counter-exchange driven by phosphoinositide turnover is not limited to OSBP but also occurs through other ORP/Osh proteins, allowing them to enrich membranes with specific lipids beyond sterol (Delfosse et al., 2020). For example, the mammalian ORP5/ORP8 subfamily (Osh6/7 in yeast) does not bind sterol but instead mediates phosphatidylserine (PS)/PI4P counter-exchange. As a result, OSBP and related ORPs play important roles in various metabolic and signaling pathways and are linked to several human diseases, including cancer and infections (Olkkonen, 2022).

A key aspect of OSBP biology is its role in viral infection, where viruses hijack its lipid-transfer activity to form intracellular viral replication organelles (Strating & van Kuppeveld, 2017). Indeed, several positive-sense single-stranded RNA viruses infecting humans, including rhinovirus, hepatitis C virus, poliovirus or Zika virus, extensively rely on OSBP to generate cholesterol-enriched membranes, which protect them from innate immune factors and promote viral replication (Amako et al., 2009; Arita et al., 2013; Roulin et al., 2014; Strating et al., 2015; Wang et al., 2014). Interestingly, targeting OSBP with inhibitory compounds blocks the

replication of several viruses. For example, natural molecules from the ORPphilin family, such as OSW-1, have shown strong inhibitory activity against the replication of dengue virus, SARS-CoV-2, and enteroviruses (Albulescu et al., 2015; Meutiawati et al., 2018; Roberts et al., 2019; Subramaniyan et al., 2025; Wang et al., 2014). Among these compounds, Macarangin B and derivatives display potent anti-Zika virus effects while exhibiting relatively low cytotoxicity (Jézéquel, Fargier, et al., 2025; Jézéquel, Grimanelli, et al., 2025).

Pharmacological and antiviral studies often focus on measurable biological effects such as viral inhibition and cytotoxicity, with ligands serving both as candidate inhibitors and as tools to probe the activity of the target protein. In this context, obtaining structural information about the protein–ligand complex offers several important advantages, as it allows direct visualization of the binding site and provides key insight into the mechanism of action. Determining the crystal structure of such a complex can be highly valuable, but technically difficult and time-consuming. By contrast, recent advances in molecular modelling, doped by AI-based structure prediction (e.g. AlphaFold (Jumper et al., 2021)) and access to supercomputer resources, allow the rapid generation of structural models and simulation of protein–ligand interactions *in silico*. These approaches, such as molecular dynamics (MD) simulations require no physical sample and can provide dynamic, mechanistic insights much faster than traditional crystallography. Notably, they allow exploration of the conformational space of both the compound and the protein over time, thereby indicating their flexibility and the stability of the interaction. In addition, MD simulations can suggest specific residues likely to be important for binding or highlight important transient contacts, which may serve as a basis for subsequent mutagenesis studies. Finally, computational approaches enable rapid *in silico* testing of analogues to predict how chemical modification might affect the interaction before synthesis.

Here we describe a protocol for setting up, running and analyzing molecular docking and MD simulations of small molecules interacting with the ORD domain of OSBP (Fig. 1A). To illustrate the procedure, we use the well-studied ORPphilin OSW-1 and the recently described Schweinfurthin-G (SW-G) and Macarangin B as example compounds (Fig. 1B) (Jézéquel, Grimanelli, et al., 2025; Péresse et al., 2020), although the protocol can be applied broadly to other protein–ligand complexes.

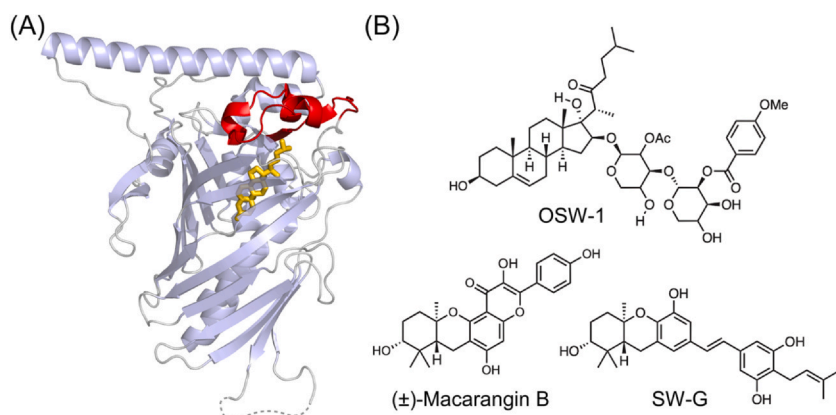


Fig. 1 Structure and compounds used for simulations. (A). Structure of OSBP ORD–cholesterol complex (PDB: 7V62). The N-terminal flexible lid region of the ORD, which covers the entrance to the hydrophobic tunnel and stabilizes the bound ligands, is colored red. Cholesterol is colored yellow. (B). Chemical structures of natural ORPphilin molecules used in this study.

2. Methods

2.1 Equipment

Workstation for bioprocessing equipped with $1 \times$ GPU, 64 GB RAM, and a 12–24 core CPU running a Linux operating system.

2.2 Before you begin

2.2.1 Molecular visualisation tools

PyMOL (<https://pymol.org/>) (Schrödinger, n.d.), and UCSF Chimera (Pettersen et al., 2004) are widely used molecular visualization tools for exploring 3D structures of macromolecules such as proteins, ligands, or nucleic acids, as well as analyzing molecular interactions. They allow users to inspect binding pockets, measure distances between atoms, visualize hydrogen bonds, modify structures (such as removing parts of the molecule, or mutate a protein residue), and also generate high-quality figures for publications. PyMOL is user-friendly, while Chimera offers more advanced analyses such as cryo-EM density maps or normal mode analysis. Here, we will focus on examples from PyMOL.

2.2.2 Experimental structures

The first step in a docking workflow consists in acquiring a reliable three-dimensional (3D) structure of the protein of interest. When the structure is available from experimental sources, it can be directly retrieved from public databases such as the Protein Data Bank (PDB) (Berman et al., 2000). Crystal structures should be preferred over NMR models, as NMR provides an ensemble of conformations, requiring a selection and therefore introducing a bias. Also, while crystallography provides high resolution structures ($\sim 1.5\text{--}2.5\text{ \AA}$), NMR structures are typically less precise (corresponding to $\sim 2.5\text{--}4.5\text{ \AA}$). Nevertheless, crystal structures should be carefully inspected since some regions might be unresolved, and mutations introduced for crystallisation may have affected the active site. When regions are missing, homology modelling or predictive approaches can be employed to complete the model (see below).

In the following example, we used the X-ray crystal structure of the ORD of human OSBP (residues 406–807) in complex with cholesterol, available under the PDB accession 7V62 (3.25 \AA resolution) (Kobayashi et al., 2022). The ORD structure consists of a 12-strand beta-barrel fold defining the lipid-binding pocket, surrounded by an N-terminal lid, which covers the entrance of the hydrophobic tunnel, and a C-terminal region comprising a long alpha helix (Fig. 1A). Prior to docking or simulation, the structure was cleaned to remove crystallographic water molecules, ions and ligands, using PyMOL (Schrödinger, n.d.).

2.2.3 Homology modelling

Experimental structures are not always available. In that case, predictive approaches must be used. The AlphaFold Protein Structure Database (Jumper et al., 2021; Varadi et al., 2022) provides structural models for all proteins listed in UniProt (The UniProt Consortium, 2021) with high confidence. Note that these structures were predicted with AlphaFold2. The most recent AlphaFold3 (Abramson et al., 2024) offers higher accuracy and the possibility to predict heteromers. Alternatively, homology modelling can be employed, in which templates are identified for the queried protein and used to generate a model. In this case, the protein sequence is first retrieved from databases such as NCBI (Sayers et al., 2023), UniProt (The UniProt Consortium, 2021), or Ensembl (Harrison et al., 2024). The closest available templates are identified through sequence alignment, and models are built using tools such as MODELLER (Fiser & Šali, 2003; Šali & Blundell, 1993), SwissModel

(Biasini et al., 2014; Schwede et al., 2003) or Rosetta (Alford et al., 2017; Song et al., 2013), provided that the sequence identity exceeds the commonly accepted threshold for homology, typically around 30 %.

2.2.4 Protein refinement

Once a 3D structure is available, it is important to determine the location of the relevant binding pocket. If this information is not known from experimental data or crystal structures, several tools can be used to identify potential binding sites, such as POCASA (Yu et al., 2009) or Protein + (Fährrolfes et al., 2017; Schöning-Stierand et al., 2020), which predict plausible binding cavities based on the protein's geometry.

In some cases, structural modifications are necessary to enable docking. For example, in the OSBP ORD structure, the presence of the lid prevents docking of large ligands such as OSW-1. Thus, the first step is to manually remove the flexible lid region (residues 413–443) from the ORD, using PyMOL, in order to expose the cavity before performing docking (click on display, sequence, select the desired atoms, right click on the selection, and select remove).

Finally, before proceeding to docking, the protein should be subjected to a short MD simulation to obtain a more relaxed and reliable structure. This helps correct potential crystal structure artifacts and compensates for inaccuracies in homology models. See below the section III. Molecular Dynamics Simulations for more detail. In addition, the GROMACS online tutorial (<http://www.mdtutorials.com/gmx/lysozyme/index.html>) is a valuable support for configuring MD simulations.

2.2.5 Small molecules preparation

If no 3D structures are available for the compounds, they can be generated from their SMILES string using online tools such as the NovoPro SMILES to PDB converter (NovoPro Lab – [smiles2pdb](#), n.d.). However, the resulting models must be carefully inspected, as incorrect chirality may be introduced. To address this, the web tool Frog2 (Miteva et al., 2010) helps generate accurate conformers of the molecule.

2.3 Step-by-step method details: Docking

2.3.1 Introduction

Molecular docking is a computational method used to predict how a small molecule, such as a ligand or drug candidate, binds to a target protein. It first emerged in the early 1980s as one of the earliest structure-based drug design

tools. The first docking program, DOCK, developed by the Kuntz's group in the 80's (Kuntz et al., 1982), used geometric sphere-matching to model how small molecules fit into protein binding pockets. Since then, docking software has significantly improved and several packages are available, each with different advantages. Widely used options include AutoDock (Steffen et al., 2010), its successor AutoDock Vina (Trott & Olson, 2009) and SwissDock (Grosdidier et al., 2011). These tools offer faster scoring function, multi-threading capabilities, and a web-based interface (e.g. MGLTools for AutoDock) that simplifies access to docking for non-specialists.

Docking algorithms generate multiple conformations of a ligand and sample their possible orientations within a target binding site. The poses are then ranked according to a scoring function, aiming to identify the most favourable interaction. The function computes contributions from van der Waals and electrostatic interactions, hydrogen bonds and solvation, to estimate the overall binding energy between the ligand and the protein. The top-ranking pose represents the likely bound conformation.

Here, we describe how to perform docking using AutoDock 4 and the interface MGLTools to study the interaction of OSBP ORD with cholesterol, OSW-1, SW-G, and the enantiomers of Macarangin B (Fig. 1B) (Jézéquel, Grimanelli, et al., 2025).

2.3.2 Required software

- OpenBabel (package for Linux)
- MGLTools (<https://ccsb.scripps.edu/mgltools/downloads/>)
- AutoDock 4 (<https://autodock.scripps.edu/download-autodock4/>)

2.3.3 Ligand and protein preparation

First, the protein structure is prepared in MGLTools by adding missing atoms, polar hydrogens, and Gasteiger charges (Fig. 2A and B). The steps below should be executed in the MGLTools window:

File – read molecule [choose the pdb protein file].

Edit – delete water.

Edit – misc – check for missing atoms – select all residues – dismiss.

Edit – misc – repair missing atoms – save as two sets – dismiss.

Edit – hydrogens – add – polar only – ok.

Edit – charges – Add Kollman Charges.

Edit – charges – Check Totals on Residues – spread charge deficit over all atoms in residue – dismiss.

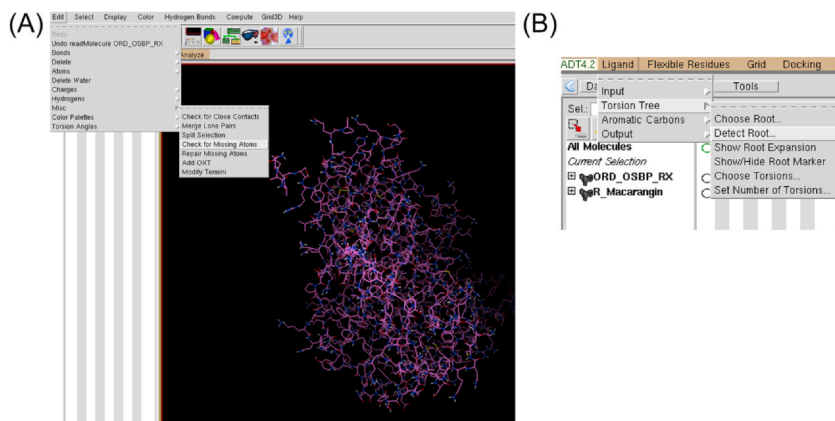


Fig. 2 Ligand and protein preparation in MGLTools. (A, B). Screenshots of the procedures to follow.

For ligand preparation, hydrogens and charges should be added, then the root of the torsion tree should be detected to define rotatable bonds. The ligand is then converted into.pdbqt format.

Ligand – input – open [choose the ligand pdb file].

Ligand – torsion tree – detect root.

Ligand – output [save as.pdbqt].

2.3.4 Box parameters

A grid box should be defined around the known binding pocket (Fig. 3A), and the corresponding gpf file saved. Alternatively, the box can be defined around the entire protein (for a “blind docking”), but this will significantly increase the computational cost.

Grid – Set Map Types – Choose Ligand, [select the ligand], *select*.

Grid – Macromolecule – Choose, [select the protein], *select*, [save as.pdbqt].

Grid – grid box [position the box by playing with the wheels].

File (of the grid options) – output grid dimensions files.

File (of the grid options) – close saving current.

Grid – output [save as.gpf].

2.3.5 Docking parameters

For OSBP ORD, docking was carried out using a population size of 300 and testing 1000 genetic algorithm runs per ligand (Fig. 3B and C). In practice, this means that the algorithm performs 1000 independent runs, each starting with 300 different initial ligand conformations that evolve

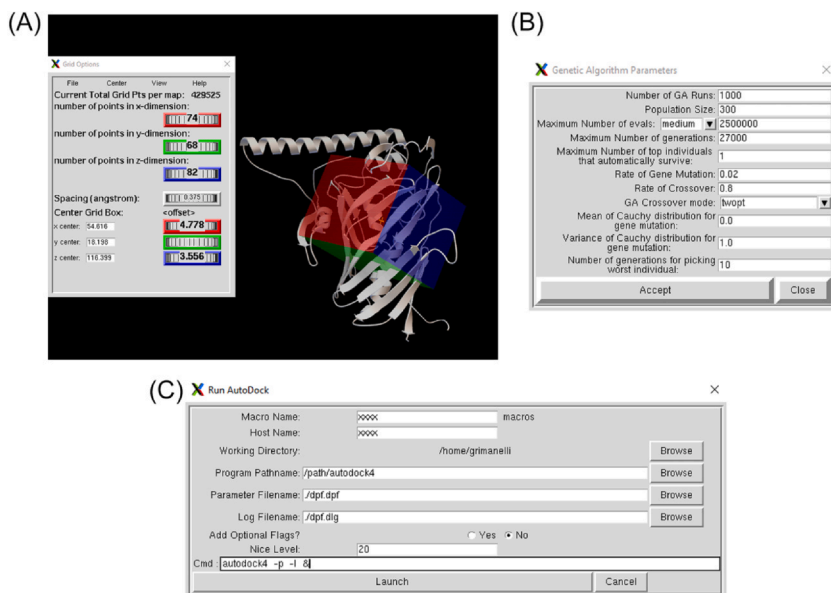


Fig. 3 Box and docking parameters in AutoDock. (A). Screenshot of the procedure to define the box around the known binding pocket of the ORD. (B, C). Screenshots of the parameters and procedure to follow to run Autodock.

during the run, to ensure thorough sampling of the conformational space. Alternatively, a population size of 150 with a few hundred runs is also acceptable. The protein is treated as rigid, while the ligand remains flexible. As mentioned before, OSW-1 docking was performed using the ORD structure lacking the lid to ensure accessibility of the lipid-binding pocket. The chosen docked conformation was later embedded into the full ORD structure including the lid, for subsequent simulations.

Docking – macromolecule – set rigid filename [choose.pdbqt of the protein].

Docking – ligand – choose, [select the ligand], *select ligand - accept*.

Docking – search parameters – genetic algorithm, [set Number of GA runs to 1000 and population size to 300], *Accept*.

Docking – output – Lamarckian GA [save.dpf file].

Run – run autogrid [input the path to autogrid4 and to the.gpf file].

Launch [wait a few seconds].

Run – autodock [input the path to autodock4 and to the.dpf file].

Launch [results are available after approximatively one day of computation].

2.3.5.1 Pose selection

Docking results are clustered and ranked based on an energy-based scoring. The lowest-energy conformation from the largest cluster is selected as the most probable binding mode (Fig. 4A). When docking simulations are performed with OSW-1, SW-G, (S)-Macarangin B or cholesterol as a control, only one large cluster of low-energy binding poses is obtained for each. By contrast, two large clusters are obtained for compound (R)-Macarangin B (Jézéquel, Grimanelli, et al., 2025).

Thereafter, visual inspection is performed to ensure chemical plausibility (Fig. 4B). If the top pose appears geometrically unrealistic or inconsistent with known binding patterns, the best pose from the next largest cluster can be considered. Note that this was not the case for all ligand tested. The following procedure should be executed: Open the docking log file (*.dlg) and look for the clustering histogram. Visualize the conformations in MGLTools (numbered as in the “run” column) and save favorite poses in.pdbqt format.

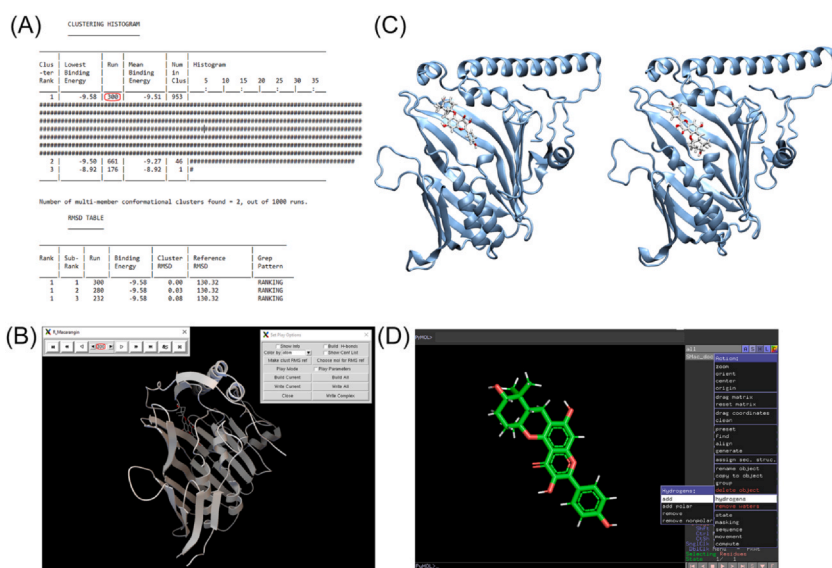


Fig. 4 Docking results and visualization. (A). Screenshot of the clustering histogram obtained from AutoDock. The cluster with the lowest binding energy is ranked first in the table. In this example, obtained with (R)-Macarangin B, two large clusters out of three are obtained, suggesting two plausible conformations. (B). Visual assessment of (R)-Macarangin B poses in AutoDock. (C). Left: ORD-(R)-Macarangin B “up”. Right: ORD-(R)-Macarangin B “down”, as visualized using VMD. (D). Screenshot of the ligand as visualized in PyMOL, and procedure to add hydrogens.

Analyze – dockings – open [choose the.dlg file].

Analyze – macromolecule – open.

Analyze – conformations – play.

& – write complex.

Interestingly, the two large clusters of low-energy binding poses determined for (R)-Macaragin B correspond to two possible orientations (“up” and “down”) within the ORD pocket (Fig. 4C). For subsequent simulations, it is recommended to perform at least three replicates per binding mode. Therefore, three similar poses from the same cluster (typically the three lowest-energy poses found in the RMSD table, Fig. 4A) should be selected and saved. If several binding modes are found in different clusters, three poses should be saved for each alternative binding mode. To retrieve only the ligand from the saved protein–ligand complex, open it with PyMOL, select the ligand, and type “save/path/to/complex/ligand.pdb, sele”.

2.3.5.2 Ligand export and visualization

Because the.pdbqt format does not preserve double bond information, visualizing the ligand directly in PyMOL may result in incorrect hydrogenation. To address this, the selected pose should be converted to.mol2 format using OpenBabel in the Linux terminal:

```
obabel ligand.pdb -O ligand.mol2.
```

This.mol2 file can then be loaded into PyMOL. Then, adding hydrogens using “Hydrogens - Add” function ensures a chemically valid representation for visualization and subsequent simulations (Fig. 4D). The results should be saved in.mol2 format.

2.3.6 Limitations

AutoDock assumes a rigid protein structure, which can limit the relevance of the results when the binding site undergoes conformational changes. Additionally, large or bulky ligands may not fit within the binding site in a rigid system. In such cases, parts of the protein may need to be removed before docking (as we did with the lid of the ORD for docking OSW-1), or the ligand may need to be splited or simplified. To account for flexibility, receptor flexibility can be modelled to some extent with tools like AutoDock Vina (Trott & Olson, 2009) or RosettaLigand (Davis & Baker, 2009), or docking can be repeated using different protein snapshots obtained from MD simulations.

2.4 Step-by-step method details: MD simulations

2.4.1 Introduction

MD is a computational technique used to explore the time-dependent behavior of biomolecules. It was first introduced in the 1950s to model phase transitions (Alder & Wainwright, 1957), and later applied to proteins in solution by McCammon, Gelin and Karplus (McCammon et al., 1977), work that ultimately contributed to the 2013 Nobel Prize in Chemistry.

In an MD simulation, a virtual box is constructed containing all atoms of the biological system. Random velocities are assigned to each atom and the algorithm then solves Newton's equation of motion to update the positions and velocities of all atoms at each timestep. This allows for the dynamic behaviour of biomolecular systems to be explored on the nanosecond to microsecond timescale. Simulations proceed through three main stages: energy minimization (to relieve steric clashes), equilibration (to stabilize the system), and production (where trajectories are collected). The equations of motion are solved using numerical algorithms such as Verlet, with the leap-frog Verlet method being the most widely used.

Periodic boundary conditions (PBC) reproduce an infinite system, which is maintained in an NPT thermodynamic ensemble (constant number of particles, pressure, and temperature). Temperature and pressure are regulated using thermostats and barostats, such as V-rescale and C-rescale, respectively.

All-atom (AA) simulations explicitly represent each atom and use a timestep of 1–2 femtoseconds, often combined with constraints (e.g., SHAKE or LINCS) to freeze covalent bonds involving hydrogen atoms, which undergo the most rapid vibrations, thereby improving efficiency. To explore the entire conformational landscape of the system, it is necessary to repeat the simulations several times with slightly different initial conditions. Running several independent replicas, rather than one long simulation, is preferable, as this maximizes the diversity of states explored by the system (Knapp et al., 2018).

MD relies on force fields, which describe the interactions between particles. They consist of a set of parameters defining the molecular topology, including terms for bonded and non-bonded interactions. Widely-used all-atom force fields include AMBER (Case et al., 2005; Case, Cheatham, et al., 2023), CHARMM (Brooks et al., 2009; Huang & Mackerell, 2013), GROMOS (Christen et al., 2005; Schmid et al., 2012; Scott et al., 1999), and OPLS-AA (Jorgensen et al., 1996; Kaminski et al., 2001), each associated

with software tools such as GROMACS (Abraham et al., 2015; Bekker et al., 1993), Amber (Case, Aktulga, et al., 2023), NAMD (Phillips et al., 2020) and LAMMPS (Thompson et al., 2022). To reduce computational cost, non-bonded interactions beyond a defined cutoff distance are ignored. Of note, although AA simulations provide detailed interaction information, they remain limited by the computational resources required (e.g., 200 ns for a 1000-residue system may require several days on a GPU). To overcome this, coarse-grained (CG) methods, such as the Martini force field, group several atoms into a single bead (Monticelli et al., 2008; Souza et al., 2021), greatly reducing the number of particles and extending the accessible timescales.

Thanks to improved hardware and the availability of user-friendly platforms such as CHARMM-GUI (Jo et al., 2008), and shared platforms such as Folding@Home (Shirts & Pande, 2000), MD simulations have become increasingly accessible and are now a valuable complement to experimental research. Below we present how to perform an all-atom MD simulation, using Gromacs 2021.3 and the charmm36 force-field, based on the procedure we followed to study the interaction between the OSBP ORD and cholesterol, SW-G, OSW-1 or (R)- and (S)-Macarangin (Jézéquel, Grimanelli, et al., 2025).

2.4.2 Required software and tools

- GROMACS
- Python
- XMGrace (<https://plasma-gate.weizmann.ac.il/pub/grace/>)
- VMD (Visual Molecular Dynamics), for visualizing and analyzing MD simulations (<https://www.ks.uiuc.edu/Development/Download/download.cgi?PackageName=VMD>)
- Simulation input files (.mdp; available here: <https://github.com/ZoeGrimanelli/Docking-and-Molecular-Dynamics-Simulations-of-ORPphilins-Targeting-OSBP>) in the working folder

2.4.3 Preparation of molecules

The first step before running MD simulations is to generate the topologies of the ligands. These files define the atomic connectivity, charges, and interaction parameters for each component of the system. The topology of small molecules can be generated from their docked conformation in.mol2 format using SwissParam (Zoete et al., 2011), a tool designed to produce

CHARMM-compatible parameters for small organic molecules. This should provide ligand.pdb and ligand.itp files.

The topology of the protein can be generated using Gromacs with the CHARMM36 force field from its.pdb. The TIP3P water model should be used, as well as the zwitterionic forms (NH_3^+ and COO^-) for the N- and C-termini, which is standard for physiological pH. Gromacs needs to be sourced first.

```
source /path/to/gromacs/GMXRC.
gmx pdb2gmx -f protein.pdb -o protein.gro -ter -ignh -p
topology.top.
```

Now, using these commands, the ligand position constraints file can be created:

```
echo -e "0 & ! a H* \n q \n" | gmx make_ndx -f ligand.pdb -o
index_lig.ndx.
echo 3 | gmx genrestr -f ligand.pdb -n index_
lig.ndx -o posre_ligand.itp -fc 1000 1000 1000.
```

To create the complex: in PyMol, open the ligand from SwissParam, select ligand and change its name in the PyMol prompt with the command line: `alter sele, resn = "LIG"`. In the ligand.itp file, rename also all "UNL1" to "LIG". Open the protein in.gro format and save the complex as complex.pdb. Open topology.top. This file contains all the necessary information for the simulation, including force field parameters of the protein and the ligand; therefore, it must be manually updated to include the ligand topology and any additional molecules introduced into the system.

At the top, after the lines:

```
;Include forcefield parameters.
#include "charmm36.ff/forcefield.itp".
```

Add:

```
;Include ligand topology.
#include "ligand.tip".
```

At the bottom, after the lines:

```
;Include Position restraint file.
#ifdef POSRES.
#include "posre.itp".
#endif.
```

Add:

```
;Ligand position restraints.
#ifdef POSRES.
#include "posre_ligand.itp".
#endif.
```

Then at the very bottom, before the line:

```
Protein_Chain_A1.
```

Add:

```
LIG1.
```

2.4.4 Minimization, equilibration, production

For each ORD/ligand system, MD simulation can now be completed with the following steps. The system is placed in a cubic simulation box with at least 2 nm between the solute and the box edges, then solvated using the SPC216 water model. The number of water molecules can be checked in the topology.top file.

```
gmx editconf -f complex.pdb -o newbox.gro -c -bt cubic -d 2.
gmx solvate -cp newbox.gro -cs spc216.gro -p topology.top -o solvate.gro.
```

Ions (NaCl or KCl) are added to neutralize the system and reach a final concentration of 120 mM; with \$nb_SOD and \$nb_CLA calculated using the formula:

$$nb_{ions} = \frac{\text{Number of water molecules} \times 0.12}{55.55} \pm counter_{ions}$$

55.55 mol/L being the molar concentration of pure water. The total charge of the system can be read from the following grompp output to determine the counter ions needed to neutralize the system. For instance, if the total charge is +5, then \$counter_ions for \$nb_CLA = 5 and for nb_SOD = 0, to add 5 negative charges.

```
gmx grompp -f ions.mdp -c solvate.gro -p topology.top -o ions.tpr.
```

```
echo SOL | gmx genion -s ions.tpr -o solv_ions.gro -p topology.top -pname SOD -np $nb_SOD -nname CLA -nn $nb_CLA.
```

Ions and water molecules surrounding the ORD within the box can be visualized by opening the file with PyMOL, and clicking show - cell (Fig. 5).

An index file can now be created:

```
gmx make_ndx -f solv_ions.gro -o index.ndx.
```

Spot the number of the groups “Protein”, “LIG”, “Water”, “SOD” and “CLA”, usually 5, 2, 16, 13, 4, respectively. Type: “5|2”, enter, “16|3|4”, enter, “q”, enter, or replace with the correct number.

The simulation workflow then follows the three preparation stages:

- Energy minimization (50,000 steps) with the -DFLEXIBLE flag
- Equilibration in the NVT ensemble for 200 ps ($\Delta t = 2$ fs),
- Followed by NPT equilibration for another 200 ps ($\Delta t = 2$ fs).

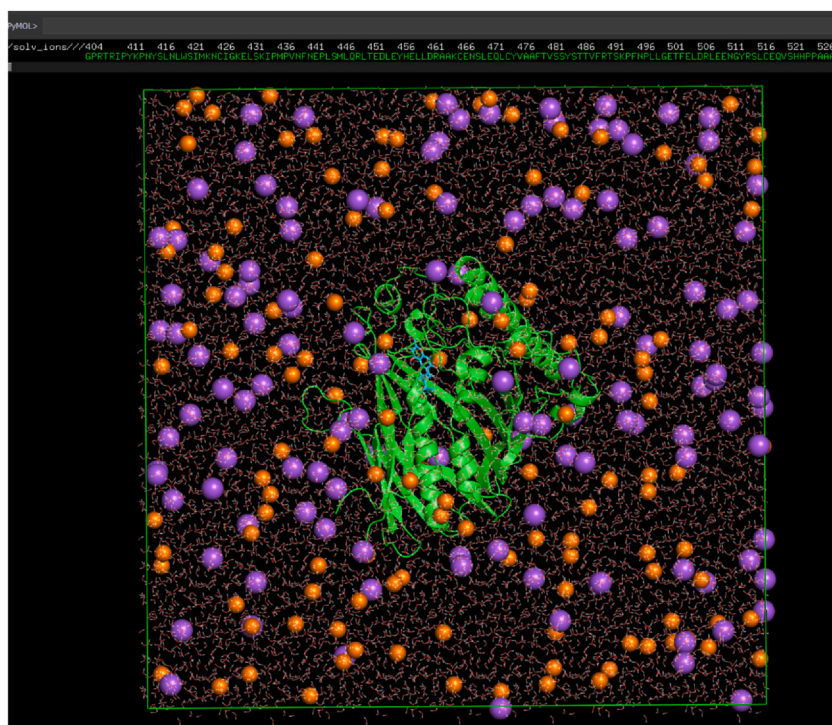


Fig. 5 Preparation of the molecules for MD simulations. Screenshot of the box containing the ORD–ligand complex surrounded by ions and water molecules in PyMOL.

The production run of each ORD–ligand complex is performed for 500 ns with a 2 fs timestep. Note that for simple protein rearrangement, 250 ns of simulation can be enough, but for a more thorough simulation or to observe events, 1 or 2 μ s might be necessary. The time of simulation can be modified in the md.mdp file with the nsteps parameter.

Temperature and pressure are controlled using two separate coupling groups: Protein–Ligand and Water–Ions. LINCS constraints are applied to bonds involving hydrogens, and Particle Mesh Ewald (PME) is used for long-range electrostatics.

```

gmx grompp -f em.mdp -c solv_ions.gro -p topology.top -o
em.tpr.
gmx mdrun -v -deffnm em.
gmx grompp -f nvt.mdp -c em.gro -r em.gro -p topo
logy.top -n index.ndx -o nvt.tpr.
gmx mdrun -deffnm nvt.
gmx grompp -f npt.mdp -c nvt.gro -t nvt.cpt -r nvt.gro -p
topology.top -n index.ndx -o npt.tpr.
gmx mdrun -deffnm npt.
gmx grompp -f md.mdp -c npt.gro -t npt.cpt -p topolo
gy.top -n index.ndx -o md.tpr.
gmx mdrun -deffnm md.

```

This last line should be executed on an adapted GPU server, with the -deffnm option modified to assign an appropriate name to the simulation outputs. The expected simulation performance is approximately 150 ns/day.

2.5 Analysis

2.5.1 Visualization of the trajectories

To prepare the trajectories, periodic boundary conditions are corrected, and water molecules are removed from one.gro file and the trajectory, to reduce file size and facilitate visualisation. The following command lines should be executed, with “Protein_LIG” specified as output. The -pbc options may be adjusted to obtain a clear visualisation, as these can be system dependant.

```

gmx trjconv -s md.tpr -f npt.gro -o npt_conv.gro -pbc mol
-n index.ndx.
gmx trjconv -s md.tpr -f md.xtc -o md_conv.xtc -pbc mol
-ur compact -n index.ndx -skip 5.

```

If multiple replicates were performed, it is possible to concatenate them into a single trajectory, as all replicates are considered to form one conformational ensemble.

```
gmx trjcat -cat -f md1_conv.xtc md2_conv.xtc  
md3_conv.xtc -o md_concat.xtc.
```

The resulting files (npt_conv.gro and md_conv.xtc) are then loaded into VMD for visualization and manual inspection. Graphical representations may be adjusted to highlight different features of interest (Fig. 6A). The trajectory can be aligned on the protein to visualize ligand motion using the following: Extensions – Analysis – RMSD trajectory tool – Align. Once an appropriate representation selected, a movie can be generated through: Extensions – Visualization – Movie maker, movie settings – trajectory. Movies illustrating the aligned trajectories during 500 ns of the complexes between OSBP ORD and cholesterol, OSW-1, SW-G, (R)-Macarangin B (up orientation), (R)-Macarangin B (down orientation) and (S)-Macarangin B are provided respectively as **Movies 1–6**. Trajectories visualization suggest that all compounds remained in the ORD binding pocket throughout the simulations.

If required, the simulation can be extended using the following commands, which should be executed on an adapted GPU server:

```
gmx convert-tptr -s md.tpr -extend 500000 -o md2.tpr.  
gmx mdrun -defnm md2 -cpi md.cpt -noappend.
```

2.5.2 RMSD and RMSF

RMSD (Root Mean Square Deviation) and RMSF (Root Mean Square Fluctuation) are two very common analysis tools. The RMSD measures the average positional deviation of atoms relative to a reference structure, providing an indicator of the system's stability over time. Variations greater than 3Å are generally considered to reflect significant conformational changes. The RMSF is a related metric calculated per residue, highlighting the regions of the molecule that exhibit the highest flexibility. These two metrics can be calculated with the following commands:

```
gmx rms -s npt_conv.gro -f md_conv.xtc -n index.ndx -tu  
ns -o rmsd.xvg.  
gmx rmsf -f md_conv.xtc -s md.tpr -o rmsf.xvg -res -b 10.
```

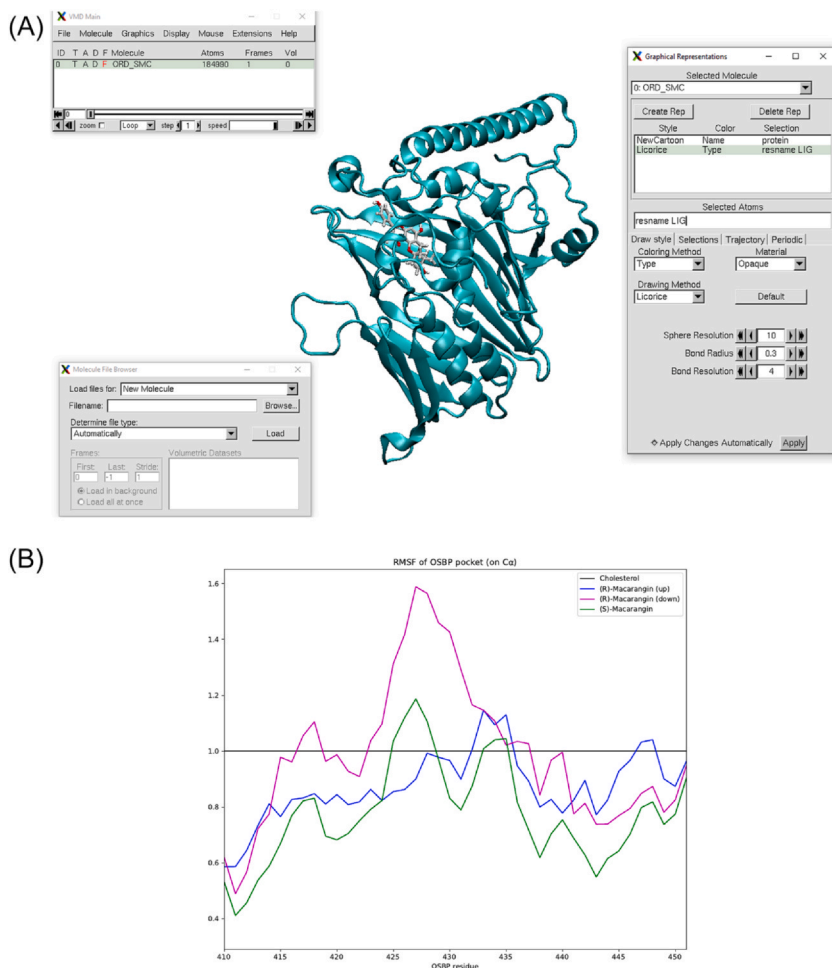


Fig. 6 Visualization and analyzes of MD simulations. (A) Screenshot of the resulting file after ORD–(S)-Macaranga B simulation using VMD. Graphical representations can be adjusted to show different features. (B) RMSF data for Ca atoms of OSBP ORD residues 410–450, measured in the presence of different compounds and normalized against the cholesterol-bound condition (represented by the black line). Values below 1 indicate greater residue stability during the MD simulation compared to the cholesterol-bound state.

Calculation may be performed on either the backbone or the C α atoms. Additional indexes can be created to calculate RMSD of specific regions, such as the binding pocket residues or the ligand, using the following command:

```
gmx make_ndx -f solv_ions.gro -n index.ndx -o index.ndx.
```

For the ligand, an index excluding hydrogens should be created to avoid artificial fluctuations due to their high vibrations, with: `LIG & a ! H*` (replace `LIG` with its corresponding number in the index, here 2). RMSD and RMSF can be visualized using `xmgrace` from the terminal. Python offers a powerful tool for customizing and processing `.xvg` files, using libraries such as `pandas` or `matplotlib`. Notably, RMSF data of selected ORD residues, in the presence of different compounds, can be normalized to those obtained with cholesterol, as illustrated in Fig. 6B, showing that both of the Macarangin B enantiomers enhance lid stability compared to cholesterol during simulation.

2.5.3 Protein ligand hydrogen bond and contact frequency

Hydrogen bonds (H-bonds) between the ligands and the protein may be analyzed over the course of the simulations, with particular attention to their occupancy, defined as the percentage of time each bond is present. H-bonds are identified using a distance cutoff of 3.5 Å and an angle cutoff of 30°, in the H-Bonds tool in VMD (Extensions – Analysis – Hydrogen Bonds). The option ‘All H-bonds’ and ‘Write output to files’ should be selected. The temporal frequency of H-bond formation can be visualized in Python, for example by generating a heatmap of occupancy (Jézéquel, Grimanelli, et al., 2025).

To evaluate broader protein–ligand interactions beyond strict H-bond criteria, protein–ligand contact frequencies can be calculated using the distance threshold of 4 Å or 6 Å. This can be performed with a VMD script (`contactFreq.tcl`), provided here: <https://github.com/ZoeGrimanelli/Docking-and-Molecular-Dynamics-Simulations-of-ORPphilins-Targeting-OSBP>. The script is executed via the VMD Tk Console, which can be accessed through Extensions – Tk console. Execution involved the commands: “`source /path/to/tcl/script`” and “`contactFreq “protein” “resname LIG”`”. This procedure generates a `contactfreq.txt` file, which can be processed and visualized as a heatmap using Python.

2.5.4 Clustering

Clustering is used to identify the most representative binding pose of each ligand throughout the simulations. The analysis is performed on the concatenated and fitted trajectory of the three replicates using the GROMOS method implemented in GROMACS:

```
gmx trjconv -f md_concat.xtc -o md_concat_fit.xtc -fit
rot+trans -n index.ndx -s md.tpr.
```

```
gmx cluster -f md_concat_fit.xtc -s md.tpr -n index.ndx
-o cluster.xpm -clndx -dist -ev -sz -method gromos -clid
-cl -g -tr -ntr -cutoff X.
```

Select “LIG” for least squares fit and RMSD-based clustering, and “Protein_LIG” for output. Set the cutoff X so that the clustering produces approximately 20 clusters. This ensures to capture differences between conformations, while avoiding excessive fragmentation. For ORD–ligand clustering, a ~ 0.05 nm cutoff is used for each ligand. Since clustering can be computationally intensive, it is recommended to test different cutoff values on a shorter trajectory, that can be obtained with:

```
gmx trjconv -f md_concat_fit.xtc -o md_concat_
fit_short.xtc -skip 50.
```

A lower cutoff results in more clusters, as even small deviations in conformation lead to the creation of separate groups. Conversely, a higher cutoff results in less clusters.

The representative structure is selected from the largest cluster, either by choosing the first structure in clusters.pdb, or by selecting a structure that exhibits specific H-bonds of interest. H-bond visualization can be performed in PyMOL by selecting the ligand and using the menu option “A – find – polar contacts – to other atoms in object”.

To verify the structure’s relevance, the clust-id.xvg file should be inspected using xmgrace: the most representative structure is expected to form an almost continuous thick black line across most of the simulation time, indicating persistent sampling within that cluster. This structure can then be used for 3D visualization and further analysis. The most representative conformations of cholesterol, OSW-1, SW-G, (*R*)-Macarangin B “up”, (*R*)-Macarangin B “down” and (*S*)-Macarangin B interacting with the ORD, as obtained from clustering the simulations of each compound, are presented in [Fig. 7](#).

2.5.5 Interaction energies

Interaction energies between each ligand and the ORD can be estimated by rerunning the MD trajectory. This procedure requires copying the original md.mdp file to a new file (md2.mdp) and appending the line energygrps = Protein LIG. A new run input file is generated and executed as follow:

```
gmx grompp -f md2.mdp -c npt.gro -t npt.cpt -p topolo-
gy.top -n index.ndx -o md2.tpr.
```

```
gmx mdrun -s md2.tpr -rerun md.xtc -e md2.edr.
```

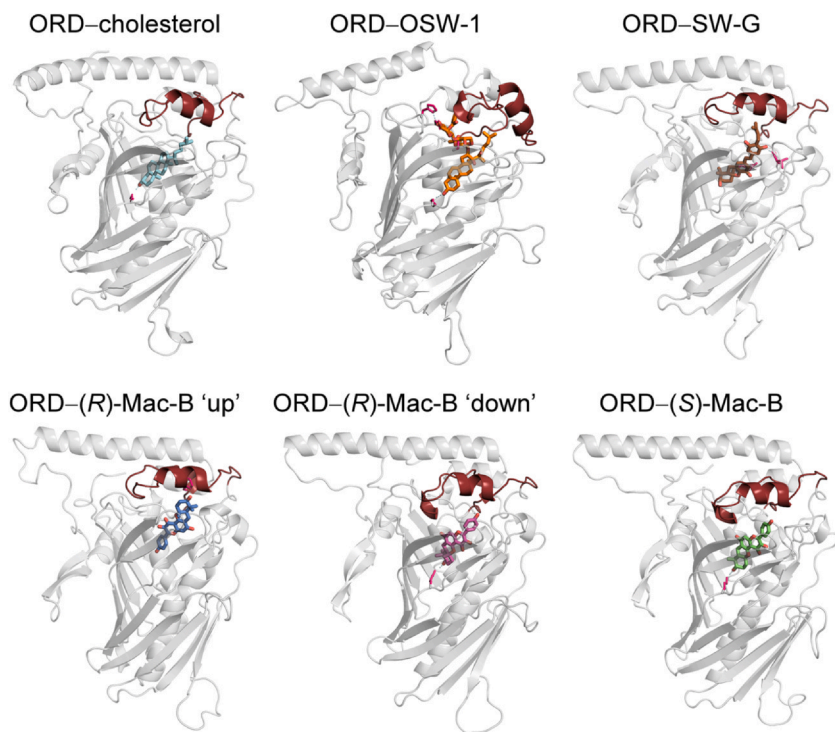


Fig. 7 ORD–Ligand clustering. Most representative binding poses of cholesterol, OSW-1, SW-G, (*R*)-Macarangenin B “up”, (*R*)-Macarangenin B “down” and (*S*)-Macarangenin B interacting with the ORD, as obtained from clustering the simulations of each compound, and illustrated using PyMOL. Residues forming frequent H-bonds with the compounds are colored pink.

Upon completion of the rerun, interaction energies are extracted from the resulting energy file using:

```
gmx energy -f md2.edr -o X.
```

Van der Waals contributions are obtained by selecting LJ-SR: Protein-LIG, and electrostatic interactions by selecting Coul-SR: Protein-LIG. The total interaction energy is then calculated as the sum of the van der Waals and electrostatic terms and can be further processed and visualized in Python to compare relative ligand binding strengths. This analysis showed similar interaction energies for cholesterol, (*R*)-Macarangenin B (both in the up or down orientations), and (*S*)-Macarangenin B within the ORD. In contrast, SW-G and especially OSW-1 should form much more stable complexes with the ORD according to their lower interaction energy (Jézéquel, Grimanelli, et al., 2025).

2.6 Limitations and validation

All-atom MD simulations are limited by timescale. Despite advances in hardware and algorithms, typical simulations span hundreds of nanoseconds to a few microseconds, which is often insufficient to capture slow or rare conformational transitions. Moreover, force field accuracy remains a key constraint, as interaction energies and structural dynamics depend on parameter sets that may not perfectly represent all molecular features, especially for unusual ligands. In addition, the reliability of results depends on sampling. Even with multiple replicates, the conformational space may not be fully explored, and clustering or energy analyzes may reflect local minima rather than global behaviour.

To validate the importance of specific binding residues identified in simulations, an *in silico* mutagenesis using PyMOL (wizard – mutagenesis – protein) can first be performed to repeat docking with the mutant proteins. For example, ORD–ligand simulations suggest that Lys577 is involved in H-bonding with cholesterol, (S)-Macaragin B, and the “down” pose of (R)-Macaragin B, whereas Phe440 forms an OH– π interaction with (R)-Macaragin B in its “up” orientation (Jézéquel, Grimanelli, et al., 2025). Thus, the corresponding ORD mutants (K577A and F440A) can be subjected to short simulations to allow structural relaxation, and then redocking as performed in part II.

Docking cholesterol into the K577A mutant should yield a larger number of clusters, including some where the headgroup is facing upward, a configuration not observed in the wild-type protein, suggesting a loss of specificity in binding. Similarly, docking (R)-Macaragin into the F440A mutant should abolish the “up” pose, etc. Whenever the results show that modifying key residues identified during MD analysis disrupts the protein–ligand interaction, they confirm their importance for binding. Nevertheless, experimental “wet lab” validation remains essential to support or refine computational findings. This includes quantitative measurements of binding affinity and binding kinetics, as well as functional assays. These assays may involve enzymatic activity assays, such as *in vitro* lipid transfer experiments, and cell-based assays, to confirm whether predicted ligand binding correlates with functional inhibition of OSBP. Similarly, mutating residues that are computationally predicted to be important for binding, and testing the resulting mutants for ligand binding or activity can be helpful for validation. In this view, MD simulations can be considered as a key hypothesis-generating tool, making experiments more interpretable.

3. Transparency statement

During the preparation of this work, the authors used ChatGPT (OpenAI) to assist in rewording some sentences to improve clarity and language. The authors reviewed and edited the content. All scientific content was generated and verified by the authors. All figures were generated by the authors.

Acknowledgements

We thank Bruno Antonny (IPMC, Valbonne) for his support, and Fanny Roussi (Institut Curie, Orsay) and Daniel Lévy (Institut Curie, Paris) for discussions. This work benefited from computing resources provided by GENCI at IDRIS on V100, H100 and A100 partitions of the supercomputer Jean Zay (Grant A0170714646), and was supported by the CNRS, Inserm, the Agence Nationale de la Recherche (ANR-21-CE13-0021-01) and the French government as part of France 2030 through the ANRS|MIE project ANRS-23-PEPR-MIE-0004. A doctoral fellowship to Z. Grimanelli was provided by Polytech Nice Sophia (Université Côte d'Azur).

Appendix A. Supporting information

Supplementary data associated with this article can be found in the online version at <https://doi.org/10.1016/bs.mie.2025.11.021>.

References

- Abraham, M. J., Murtola, T., Schulz, R., Páll, S., Smith, J. C., Hess, B., & Lindahl, E. (2015). GROMACS: High performance molecular simulations through multi-level parallelism from laptops to supercomputers. *SoftwareX*, 1–2, 19–25. <https://doi.org/10.1016/j.softx.2015.06.001>.
- Abramson, J., Adler, J., Dunger, J., Evans, R., Green, T., Pritzel, A., ... Jumper, J. M. (2024). Accurate structure prediction of biomolecular interactions with AlphaFold 3. *Nature*, 630(8016), 493–500. <https://doi.org/10.1038/s41586-024-07487-w>.
- Albulescu, L., Strating, J. R. P. M., Thibaut, H. J., Van Der Linden, L., Shair, M. D., Neyts, J., & Van Kuppeveld, F. J. M. (2015). Broad-range inhibition of enterovirus replication by OSW-1, a natural compound targeting OSBP. *Antiviral Research*, 117. <https://doi.org/10.1016/j.antiviral.2015.02.013>.
- Alder, B. J., & Wainwright, T. E. (1957). Phase transition for a hard sphere system. *The Journal of Chemical Physics*, 27(5), <https://doi.org/10.1063/1.1743957>.
- Alford, R. F., Leaver-Fay, A., Jeliaskov, J. R., O'Meara, M. J., DiMaio, F. P., Park, H., ... Gray, J. J. (2017). The Rosetta all-atom energy function for macromolecular modeling and design. *Journal of Chemical Theory and Computation*, 13(6), <https://doi.org/10.1021/acs.jctc.7b00125>.
- Amako, Y., Sarkeshik, A., Hotta, H., Yates, J., & Siddiqui, A. (2009). Role of oxysterol binding protein in hepatitis C virus infection. *Journal of Virology*, 83(18), <https://doi.org/10.1128/jvi.00958-09>.
- Appu, A. P., Bagh, M. B., Plavelil, N., Mondal, A., Sadhukhan, T., Singh, S. P., ... Mukherjee, A. B. (2025). Niemann Pick C1 mistargeting disrupts lysosomal cholesterol homeostasis contributing to neurodegeneration in a Batten disease model. *Science Advances*, 11(19), eadr5703. <https://doi.org/10.1126/sciadv.adr5703>.

- Arita, M., Kojima, H., Nagano, T., Okabe, T., Wakita, T., & Shimizu, H. (2013). Oxysterol-binding protein family I is the target of minor enviroxime-like compounds. *Journal of Virology*, 87(8), <https://doi.org/10.1128/jvi.03546-12>.
- Bekker, H., Berendsen, H., Dijkstra, E. J., Achterop, S., Drunen, R., van der Spoel, D., ... Renardus, M. K. R. (1993). Gromacs: A parallel computer for molecular dynamics simulations. *Physics Computing*, 92, 252–256.
- Berman, H. M., Westbrook, J., Feng, Z., Gilliland, G., Bhat, T. N., Weissig, H., ... Bourne, P. E. (2000). The protein Data Bank. *Nucleic Acids Research*, 28(1), <https://doi.org/10.1093/nar/28.1.235>.
- Biasini, M., Bienert, S., Waterhouse, A., Arnold, K., Studer, G., Schmidt, T., ... Schwede, T. (2014). SWISS-MODEL: Modelling protein tertiary and quaternary structure using evolutionary information. *Nucleic Acids Research*, 42(W1), <https://doi.org/10.1093/nar/gku340>.
- Brooks, B. R., Brooks, C. L., Mackerell, A. D., Nilsson, L., Petrella, R. J., Roux, B., ... Karplus, M. (2009). CHARMM: The biomolecular simulation program. *Journal of Computational Chemistry*, 30(10), <https://doi.org/10.1002/jcc.21287>.
- Case, D. A., Aktulga, H. M., Belfon, K., Cerutti, D. S., Cisneros, G. A., Cruzeiro, V. W. D., ... Merz, K. M. (2023). AmberTools. *Journal of Chemical Information and Modeling*, 63(20), <https://doi.org/10.1021/acs.jcim.3c01153>.
- Case, D. A., Cheatham, T. E., Darden, T., Gohlke, H., Luo, R., Merz, K. M., ... Woods, R. J. (2005). The Amber biomolecular simulation programs. *Journal of Computational Chemistry*, 26(16), <https://doi.org/10.1002/jcc.20290>.
- Case, D.A., Cheatham, T.E.I., Simmerling, C., Roitberg, A., Merz, K.M., Walker, R.C., & Kollman, P.A. (2023). Amber 2023. University of California, San Francisco.
- Christen, M., Hünenberger, P. H., Bakowies, D., Baron, R., Bürgi, R., Geerke, D. P., ... Van Gunsteren, W. F. (2005). The GROMOS software for biomolecular simulation: GROMOS05. *Journal of Computational Chemistry*, 26(16), <https://doi.org/10.1002/jcc.20303>.
- Davis, I. W., & Baker, D. (2009). RosettaLigand Docking with full ligand and receptor flexibility. *Journal of Molecular Biology*, 385(2), <https://doi.org/10.1016/j.jmb.2008.11.010>.
- de la Mora, E., Dezi, M., Di Cicco, A., Bigay, J., Gautier, R., Manzi, J., ... Lévy, D. (2021). Nanoscale architecture of a VAP-A–OSBP tethering complex at membrane contact sites. *Nature Communications*, 12(1), 3459. <https://doi.org/10.1038/s41467-021-23799-1>.
- Delfosse, V., Bourguet, W., & Drin, G. (2020). Structural and functional specialization of OSBP-related proteins. *Contact*, 3, <https://doi.org/10.1177/2515256420946627>.
- Fährrolfes, R., Bietz, S., Flachsenberg, F., Meyder, A., Nittinger, E., Otto, T., ... Rarey, M. (2017). Proteins plus: A web portal for structure analysis of macromolecules. *Nucleic Acids Research*, 45(W1), <https://doi.org/10.1093/nar/gkx333>.
- Fiser, A., & Šali, A. (2003). MODELLER: Generation and refinement of homology-based protein structure models. *Methods in Enzymology*, 374, [https://doi.org/10.1016/S0076-6879\(03\)74020-8](https://doi.org/10.1016/S0076-6879(03)74020-8).
- Grosdidier, A., Zoete, V., & Michielin, O. (2011). SwissDock, a protein–small molecule docking web service based on EADock DSS. *Nucleic Acids Research*, 39(2), <https://doi.org/10.1093/nar/gkr366>.
- Harrison, P. W., Amode, M. R., Austine-Orimoloye, O., Azov, A. G., Barba, M., Barnes, I., ... Yates, A. D. (2024). Ensembl 2024. *Nucleic Acids Research*, 52(D1), <https://doi.org/10.1093/nar/gkad1049>.
- Huang, J., & Mackerell, A. D. (2013). CHARMM36 all-atom additive protein force field: Validation based on comparison to NMR data. *Journal of Computational Chemistry*, 34(25), <https://doi.org/10.1002/jcc.23354>.

- Jézéquel, G., Fargier, J., Bigay, J., Polidori, J., Geslin, J., Hue, N., ... Roussi, F. (2025). Analogues of natural macaragin B display potent antiviral activity and better metabolic stability. *ChemMedChem*, 20(9), e202400978. <https://doi.org/10.1002/cmdc.202400978>.
- Jézéquel, G., Grimanelli, Z., Guimard, C., Bigay, J., Haddad, J., Bignon, J., ... Roussi, F. (2025). Minimalist natural ORPphilin macaragin B delineates OSBP biological function. *Journal of Medicinal Chemistry*, 68(1), 196–211. <https://doi.org/10.1021/acs.jmedchem.4c01705>.
- Jo, S., Kim, T., Iyer, V. G., & Im, W. (2008). CHARMM-GUI: A web-based graphical user interface for CHARMM. *Journal of Computational Chemistry*, 29(11), <https://doi.org/10.1002/jcc.20945>.
- Jorgensen, W. L., Maxwell, D. S., & Tirado-Rives, J. (1996). Development and testing of the OPLS all-atom force field on conformational energetics and properties of organic liquids. *Journal of the American Chemical Society*, 118(45), <https://doi.org/10.1021/ja9621760>.
- Jumper, J., Evans, R., Pritzel, A., Green, T., Figurnov, M., Ronneberger, O., ... Hassabis, D. (2021). Highly accurate protein structure prediction with AlphaFold. *Nature*, 596(7873), 583–589. <https://doi.org/10.1038/s41586-021-03819-2>.
- Kaminski, G. A., Friesner, R. A., Tirado-Rives, J., & Jorgensen, W. L. (2001). Evaluation and reparametrization of the OPLS-AA force field for proteins via comparison with accurate quantum chemical calculations on peptides. *Journal of Physical Chemistry B*, 105(28), <https://doi.org/10.1021/jp003919d>.
- Knapp, B., Ospina, L., & Deane, C. M. (2018). Avoiding false positive conclusions in molecular simulation: The importance of replicas. *Journal of Chemical Theory and Computation*, 14(12), <https://doi.org/10.1021/acs.jctc.8b00391>.
- Kobayashi, J., Arita, M., Sakai, S., Kojima, H., Senda, M., Senda, T., ... Kato, R. (2022). Ligand recognition by the lipid transfer domain of human OSBP is important for enterovirus replication. *ACS Infectious Diseases*, 8(6), 1161–1170. <https://doi.org/10.1021/acsinfecdis.2c00108>.
- Kovács, D., Gay, A. S., Debayle, D., Abélanet, S., Patel, A., Mesmin, B., ... Antonny, B. (2024). Lipid exchange at ER–trans-Golgi contact sites governs polarized cargo sorting. *Journal of Cell Biology*, 223(1), <https://doi.org/10.1083/jcb.202307051>.
- Kuntz, I. D., Blaney, J. M., Oatley, S. J., Langridge, R., & Ferrin, T. E. (1982). A geometric approach to macromolecule–ligand interactions. *Journal of Molecular Biology*, 161(2), [https://doi.org/10.1016/0022-2836\(82\)90153-X](https://doi.org/10.1016/0022-2836(82)90153-X).
- Lim, C. Y., Davis, O. B., Shin, H. R., Zhang, J., Berdan, C. A., Jiang, X., ... Zoncu, R. (2019). ER–lysosome contacts enable cholesterol sensing by mTORC1 and drive aberrant growth signalling in Niemann–Pick type C. *Nature Cell Biology*, 21(10), <https://doi.org/10.1038/s41556-019-0391-5>.
- Malek, M., Wawrzyniak, A. M., Koch, P., Lüchtenborg, C., Hessenberger, M., Sachsenheimer, T., ... Haucke, V. (2021). Inositol triphosphate-triggered calcium release blocks lipid exchange at endoplasmic reticulum–Golgi contact sites. *Nature Communications*, 12(1), <https://doi.org/10.1038/s41467-021-22882-x>.
- McCammon, J. A., Gelin, B. R., & Karplus, M. (1977). Dynamics of folded proteins. *Nature*, 267(5612), <https://doi.org/10.1038/267585a0>.
- Mesmin, B., Bigay, J., Moser Von Filseck, J., Lacas-Gervais, S., Drin, G., & Antonny, B. (2013). A four-step cycle driven by PI(4)P hydrolysis directs sterol/PI(4)P exchange by the ER–Golgi Tether OSBP. *Cell*, 155(4), <https://doi.org/10.1016/j.cell.2013.09.056>.
- Mesmin, B., Bigay, J., Polidori, J., Jamecna, D., Lacas-Gervais, S., & Antonny, B. (2017). Sterol transfer, PI 4P consumption, and control of membrane lipid order by endogenous OSBP. *The EMBO Journal*, 36(21), <https://doi.org/10.15252/embj.201796687>.
- Meutiawati, F., Bezemer, B., Strating, J. R. P. M., Overheul, G. J., Žusinaite, E., van Kuppeveld, F. J. M., ... van Rij, R. P. (2018). Posaconazole inhibits dengue virus replication by targeting oxysterol-binding protein. *Antiviral Research*, 157. <https://doi.org/10.1016/j.antiviral.2018.06.017>.

- Miteva, M. A., Guyon, F., & Tufféry, P. (2010). Frog2: Efficient 3D conformation ensemble generator for small compounds. *Nucleic Acids Research*, 38(2), <https://doi.org/10.1093/nar/gkq325>.
- Monticelli, L., Kandasamy, S. K., Periole, X., Larson, R. G., Tieleman, D. P., & Marrink, S. J. (2008). The MARTINI coarse-grained force field: Extension to proteins. *Journal of Chemical Theory and Computation*, 4(5), <https://doi.org/10.1021/ct700324x>.
- NovoPro Lab - smiles2pdb. (n.d.). Retrieved 27 August 2023 from <https://www.novoprolabs.com/tools/smiles2pdb>.
- Olkkonen, V. M. (2022). The emerging roles of OSBP-related proteins in cancer: Impacts through phosphoinositide metabolism and protein–protein interactions. *Biochemical Pharmacology*, 196. <https://doi.org/10.1016/j.bcp.2021.114455>.
- Olkkonen, V. M., & Ikonen, E. (2024). Getting to grips with the oxysterol-binding protein family – a forty year perspective. *Contact (Thousand Oaks (Ventura County, Calif.))*, 7. <https://doi.org/10.1177/25152564241273598> 25152564241273600.
- Péresse, T., Kovacs, D., Subra, M., Bigay, J., Tsai, M. C., Polidori, J., ... Mesmin, B. (2020). Molecular and cellular dissection of the oxysterol-binding protein cycle through a fluorescent inhibitor. *Journal of Biological Chemistry*, 295(13), <https://doi.org/10.1074/jbc.RA119.012012>.
- Pettersen, E. F., Goddard, T. D., Huang, C. C., Couch, G. S., Greenblatt, D. M., Meng, E. C., & Ferrin, T. E. (2004). UCSF Chimera—a visualization system for exploratory research and analysis. *Journal of Computational Chemistry*, 25(13), 1605–1612. <https://doi.org/10.1002/jcc.20084>.
- Phillips, J. C., Hardy, D. J., Maia, J. D. C., Stone, J. E., Ribeiro, J. V., Bernardi, R. C., ... Luthey-Schulten, Z., ... Tajkhorshid, E. (2020). Scalable molecular dynamics on CPU and GPU architectures with NAMD. *Journal of Chemical Physics*, 153(4), <https://doi.org/10.1063/5.0014475>.
- Roberts, B. L., Severance, Z. C., Bensen, R. C., Le, A. T., Kothapalli, N. R., Nuñez, J. I., ... Burgett, A. W. G. (2019). Transient compound treatment induces a multigenerational reduction of oxysterol-binding protein (OSBP) levels and prophylactic antiviral activity. *ACS Chemical Biology*, 14(2), <https://doi.org/10.1021/acschembio.8b00984>.
- Roulin, P. S., Lötzerich, M., Torta, F., Tanner, L. B., Van Kuppeveld, F. J. M., Wenk, M. R., & Greber, U. F. (2014). Rhinovirus uses a phosphatidylinositol 4-phosphate/cholesterol counter-current for the formation of replication compartments at the ER–Golgi interface. *Cell Host and Microbe*, 16(5), <https://doi.org/10.1016/j.chom.2014.10.003>.
- Šali, A., & Blundell, T. L. (1993). Comparative protein modelling by satisfaction of spatial restraints. *Journal of Molecular Biology*, 234(3), <https://doi.org/10.1006/jmbi.1993.1626>.
- Sayers, E. W., Bolton, E. E., Brister, J. R., Canese, K., Chan, J., Comeau, D. C., ... Sherry, S. T. (2023). Database resources of the national center for biotechnology information in 2023. *Nucleic Acids Research*, 51(D1), <https://doi.org/10.1093/nar/gkac1032>.
- Schmid, N., Christ, C. D., Christen, M., Eichenberger, A. P., & Van Gunsteren, W. F. (2012). Architecture, implementation and parallelisation of the GROMOS software for biomolecular simulation. *Computer Physics Communications*, 183(4), <https://doi.org/10.1016/j.cpc.2011.12.014>.
- Schöning-Stierand, K., Diedrich, K., Fährrolfes, R., Flachsenberg, F., Meyder, A., Nittinger, E., ... Rarey, M. (2020). ProteinsPlus: Interactive analysis of protein–ligand binding interfaces. *Nucleic Acids Research*, 48(W1), <https://doi.org/10.1093/NAR/GKAA235>.
- Schrödinger L.L.C. (n.d.). PyMOL Molecular Graphics System (2.5).
- Schwede, T., Kopp, J., Guex, N., & Peitsch, M. C. (2003). SWISS-MODEL: An automated protein homology-modeling server. *Nucleic Acids Research*, 31(13), <https://doi.org/10.1093/nar/gkg520>.

- Scott, W. R. P., Hünenberger, P. H., Tironi, I. G., Mark, A. E., Billeter, S. R., Fennen, J., ... Van Gunsteren, W. F. (1999). The GROMOS biomolecular simulation program package. *Journal of Physical Chemistry A*, 103(19), <https://doi.org/10.1021/jp984217f>.
- Shirts, M., & Pande, V. S. (2000). Screen savers of the world unite. *Science*, 290(5498), <https://doi.org/10.1126/science.290.5498.1903>.
- Song, Y., Dimaio, F., Wang, R. Y. R., Kim, D., Miles, C., Brunette, T., ... Baker, D. (2013). High-resolution comparative modeling with RosettaCM. *Structure (London, England: 1993)*, 21(10), <https://doi.org/10.1016/j.str.2013.08.005>.
- Souza, P. C. T., Alessandri, R., Barnoud, J., Thallmair, S., Faustino, I., Grünewald, F., ... Marrink, S. J. (2021). Martini 3: A general purpose force field for coarse-grained molecular dynamics. *Nature Methods*, 18(4), <https://doi.org/10.1038/s41592-021-01098-3>.
- Steffen, C., Thomas, K., Huniar, U., Hellweg, A., Rubner, O., & Schroer, A. (2010). AutoDock4 and AutoDockTools4: Automated docking with selective receptor flexibility. *Journal of Computational Chemistry*, 31(16).
- Strating, J. R. P. M., van der Linden, L., Albulescu, L., Bigay, J., Arita, M., Delang, L., ... DeMatteis, M. A., ... van Kuppeveld, F. J. M. (2015). Itraconazole inhibits enterovirus replication by targeting the oxysterol-binding protein. *Cell Reports*, 10(4), <https://doi.org/10.1016/j.celrep.2014.12.054>.
- Strating, J. R., & van Kuppeveld, F. J. (2017). Viral rewiring of cellular lipid metabolism to create membranous replication compartments. *Current Opinion in Cell Biology*, 47, <https://doi.org/10.1016/j.celb.2017.02.005>.
- Subramaniam, B., Falcon, E. C., Moore, A. R., Larabee, J. L., Nimmo, S. L., Berrios-Rivera, J. L., ... Burgett, A. W. G. (2025). Anti-SARS-CoV-2 small molecule targeting of oxysterol-binding protein (OSBP) activates cellular antiviral innate immunity. *ACS Infectious Diseases*, 11(5), 1064–1077. <https://doi.org/10.1021/acsinfecdis.4c00631>.
- Tan, J. X., & Finkel, T. (2022). A phosphoinositide signalling pathway mediates rapid lysosomal repair. *Nature*, 609(7928), <https://doi.org/10.1038/s41586-022-05164-4>.
- The UniProt Consortium (2021). UniProt: The universal protein knowledgebase in 2021. *Nucleic Acids Research*, 49(D1), D480–D489. <https://doi.org/10.1093/nar/gkaa1100>.
- Thompson, A. P., Aktulga, H. M., Berger, R., Bolintineanu, D. S., Brown, W. M., Crozier, P. S., ... Plimpton, S. J. (2022). LAMMPS – a flexible simulation tool for particle-based materials modeling at the atomic, meso, and continuum scales. *Computer Physics Communications*, 271, <https://doi.org/10.1016/j.cpc.2021.108171>.
- Trott, O., & Olson, A. J. (2009). AutoDock Vina: Improving the speed and accuracy of docking with a new scoring function, efficient optimization, and multithreading. *Journal of Computational Chemistry*, <https://doi.org/10.1002/jcc.21334>.
- Varadi, M., Anyango, S., Deshpande, M., Nair, S., Natassia, C., Yordanova, G., ... Velankar, S. (2022). AlphaFold protein structure database: Massively expanding the structural coverage of protein-sequence space with high-accuracy models. *Nucleic Acids Research*, 50(D1), <https://doi.org/10.1093/nar/gkab1061>.
- Wang, H., Perry, J. W., Lauring, A. S., Neddermann, P., De Francesco, R., & Tai, A. W. (2014). Oxysterol-binding protein is a phosphatidylinositol 4-kinase effector required for HCV replication membrane integrity and cholesterol trafficking. *Gastroenterology*, 146(5), 1311–1373. <https://doi.org/10.1053/j.gastro.2014.02.002>.
- Yu, J., Zhou, Y., Tanaka, I., & Yao, M. (2009). Roll: A new algorithm for the detection of protein pockets and cavities with a rolling probe sphere. *Bioinformatics (Oxford, England)*, 26(1), <https://doi.org/10.1093/bioinformatics/btp599>.
- Zoete, V., Cuendet, M. A., Grosdidier, A., & Michielin, O. (2011). SwissParam: A fast force field generation tool for small organic molecules. *Journal of Computational Chemistry*, 32(11), <https://doi.org/10.1002/jcc.21816>.